Theoretical efficiency of Hybrid Solar Thermoelectric-Photovoltaic Generators

Bruno Lorenzi[1, 2, *] and Gang Chen[2]

[1] *Department of Materials Science, University of Milano-Bicocca, I-20125 Milan, Italy*
[2] *Mechanical Engineering Department, Massachusetts Institute of Technology, Cambridge, Massachusetts 02139, USA*

(Dated: May 9, 2018)

This work analyses the potential of hybrid solar thermoelectric photovoltaic generators (HSTEPVGs) through evaluating their efficiency in converting solar power into electricity for a system consisting of a PV cell placed directly on top of a thermoelectric generator. A theoretical model for terrestrial application which includes the possibility of thermal and optical concentrations is reported. As in the case of pure solar thermoelectric generators (STEGs), an optimal operation temperature also exists for HSTEPVGs determined by the temperature dependences of both the solar cells and the thermoelectric generators. The study reports efficiency gain of 4-5% with respect to the sole PV case, especially in the case of optical concentrations which mitigate the solar cell temperature sensitivity. In addition to these interesting results, the work also reveals the major constrains expected for this approach, along with technological challenges especially regarding the optical properties of the device encapsulation and the solar cell degradation.

I. INTRODUCTION

Photovoltaics (PV) solar energy harvesting represents one of the most dominant ways of producing electrical power with renewable resources. In this field silicon solar cells are the mainstream solution, holding more than the 90% of the market. However, it is well know that single-junction solar cells are bound to a maximum conversion efficiency of ≈33%, by the Shockley and Quisser (SQ) limit. Recently many efforts have been dedicated to the testing of different technologies promising to overcome this limit through the exploitation of the entire solar spectrum. Among them the most popular are tandem, and multi-junctions devices in which different materials convert different parts of the solar spectrum [1]. More recently the possibility of converting the whole solar spectrum via thermal conversion has attracted attention, especially with the advent of nanotechnology. Examples of this approach are thermophotovoltaics (TPV) [2, 3] and solar thermoelectric generators (STEG) [4, 5]. However, the still relatively low energy-conversion efficiencies reported for these kind of systems have so far limited their possible commercialization.

An intermediate viable solution comes from the so-called hybrid solar thermoelectric photovoltaic generators (HSTEPVG) which promise to take advantages from both the tandem and the thermal conversion approaches. Two main solutions have been reported in this field. The first is the spectrum splitting (or optically coupled) approach in which a beam splitter is used in order to direct the part of the solar spectrum with high energy onto the solar cell, and the infrared part on a thermoelectric generator (TEG). The potential of this approach was studied theoretically in the last ten years by different groups with interesting results [6–9].

The second consists instead of the direct thermal coupling between the two components, in which the TEG is placed underneath the solar cell, in thermal contact with it. In addition theoretical models often reported efficiencies higher than the sole PV case for this approach. However, most of these studies were focused on particular cases with no attempt to evaluate the generic potential of the hybrid approach [10–16]. Rarely the solar cell and the thermoelectric part have been described in general terms through their fundamental parameters [17]. However also in this case the model was intended to evaluate the theoretical limit in a SQ-like study, without taking into account the limits of current materials.

In the absence of a systematic work evaluating the potential of HSTEPVG systems with state of the art technologies, we report here a study intended to cover this gap. In this work we propose a theoretical model to the predict the efficiency of a generic HSTEPVG for terrestrial applications, with and without optical concentration. The results show that the efficiency gain due to TEG addition can be as high as 4-5% of the solar power for little or no optical concentration. The gain was found to increase for higher concentration ratio due to its beneficial effect on the solar cell temperature sensitivity. The analysis also addresses the fundamental importance of the encapsulation optical properties, along with the crucial and delicate matter of the optimal working temperature.

II. THEORETICAL MODEL

In this work we consider an unit cell of a generic hybrid solar thermoelectric-photovoltaic generator (HSTEPVG) as that shown in Fig. 1. In this system a photovoltaic (PV) cell is placed in thermal contact, but electrically isolated from a couple of p and n type thermoelectric materials. For the sake of simplicity here we will consider the case of a thermoelectric generator (TEG) composed only by a couple, but as we will show later, under the assumption of this model, the number of couples (N_c) does not influence the maximum achievable efficiency

*Corresponding author. E–mail: bruno.lorenzi@unimib.it

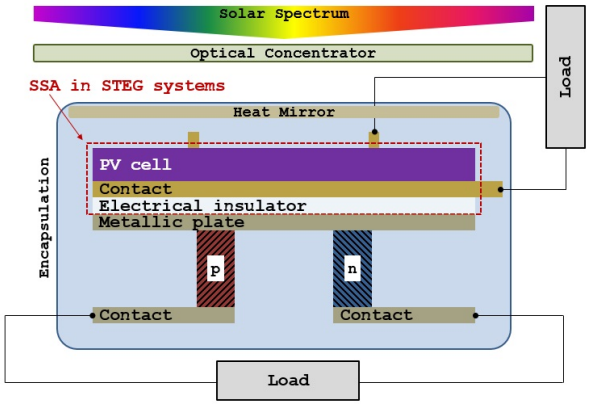

FIG. 1: The assemble of a generic HSTEPVG system where the PV cell is placed in thermal contact with the TEG, but separated from an electrical point of view. The dashed red square highlights the components which substitute the SSA in comparison with a STEG system. The other additional component is the so-called Heat Mirror, used in order to prevent radiative heat dissipation towards the environment.

of the hybrid device. The unit cell is encapsulated within an evacuated environment reducing convective heat exchange with the exterior. The encapsulation top internal surface is provided with an additional component, so-called Heat Mirror (HM), used in order to prevent radiative heat dissipation, as will be discussed in detail later. The HSTEPVG reported in Fig. 1 can be seen as a solar thermoelectric generator STEG [18] in which the solar selective absorber (SSA) is substituted by a photovoltaic cell.

In this work we will make an evaluation of the theoretical maximum achievable efficiency of the HSTEPVG unit cell of Fig. 1 under the following assumptions:
1) The system is supposed to work in a terrestrial environment therefore the ambient temperature T_a=300 K is taken as fixed, and the solar irradiance is that of the A.M. 1.5 solar spectrum with a total power density G=1000 W/m^2.
2) The PV cell is assumed to be at uniform temperature T_h equal to that of the TEG hot side.
3) The thermoelectric properties of the TEG are independent from temperature.
4) Electrical and thermal contact resistance are negligible.
5) Lateral heat exchange from the side walls of the thermoelectric elements are negligible.

A. Thermal model

As already reported by Chen [19], the energy balance for a STEG system is

$$P_\mathrm{in}^\mathrm{steg} = Q_\mathrm{te} + Q_\mathrm{con} + Q_\mathrm{rad} \tag{1}$$

with $P_\mathrm{in}^\mathrm{steg}$ the solar power, Q_te the heat flowing through the TEG, and Q_con and Q_rad respectively the heat lost towards the environment by convection, and radiation. The incoming power $P_\mathrm{in}^\mathrm{steg}$ can be written as

$$P_\mathrm{in}^\mathrm{steg} = \gamma_\mathrm{op}\eta_\mathrm{op}\tau_\mathrm{enc}\alpha_\mathrm{abs}GA_\mathrm{abs} \tag{2}$$

where γ_op, and η_op are respectively the optical concentration ratio, and the efficiency of the optical system in concentrating the light, τ_enc the encapsulation transmittance, α_abs the SSA absorbance, G the solar power, and A_abs the absorber area.
In the case of HSTEPVG systems some of the incoming power is converted in useful electrical power by the solar cell. In addition the metallic contact grid on the top of the solar device creates a shadowing effect reducing the incoming power. The remaining part is emitted back to the outside (a minor contribution which contributes to the reflectance spectra), or it is converted by different kind of losses in thermal power, as reported by several works [3, 20–23].
Therefore the power available for the TEG in the case of a HSTEPVG system can be written as

$$P_\mathrm{in}^\mathrm{hstepvg} = \eta_\mathrm{th}\gamma_\mathrm{op}\eta_\mathrm{op}GA_\mathrm{abs} \tag{3}$$

where η_th is the PV efficiency in converting the incoming power into usable heat

$$\eta_\mathrm{th} = (1-\eta_\mathrm{pv})(1-r)(1-s)\tau_\mathrm{enc} = (1-\eta_\mathrm{pv})\eta_\mathrm{opt} \tag{4}$$

with η_pv, r, and s are respectively the PV cell efficiency, reflectance and shadowing loss ratios. In Eq. 4 we have grouped the contributions of r and s under the the optical efficiency η_opt.

$$\eta_\mathrm{opt} = (1-r)(1-s)\tau_\mathrm{enc} \tag{5}$$

As we defined an efficiency in converting the incoming power into usable thermal power (η_th), we can also define an efficiency within which the heat is lost towards the environment as

$$\eta_\mathrm{th-loss} = \frac{Q_\mathrm{con}+Q_\mathrm{rad}}{\gamma_\mathrm{op}GA_\mathrm{abs}} \tag{6}$$

The reason of the definition of $\eta_\mathrm{th-loss}$ will be clear in the next section.
The convective component of the heat lost towards the environment Q_con can be written as

$$Q_\mathrm{con} = \frac{T_\mathrm{h}-T_\mathrm{c}}{R_\mathrm{con}} \tag{7}$$

where R_con is the convective thermal resistance between the HSTEPVG unit cell and the environment. The radiative contribution is instead

$$Q_\mathrm{rad} = \varepsilon_\mathrm{pv}^\mathrm{up}\sigma A_\mathrm{abs}(T_\mathrm{h}^4 - T_\mathrm{a}^4) + \varepsilon_\mathrm{pv}^\mathrm{down}\sigma\left(A_\mathrm{abs}-A_\mathrm{teg}\right)\left(T_\mathrm{h}^4-T_\mathrm{c}^4\right) \tag{8}$$

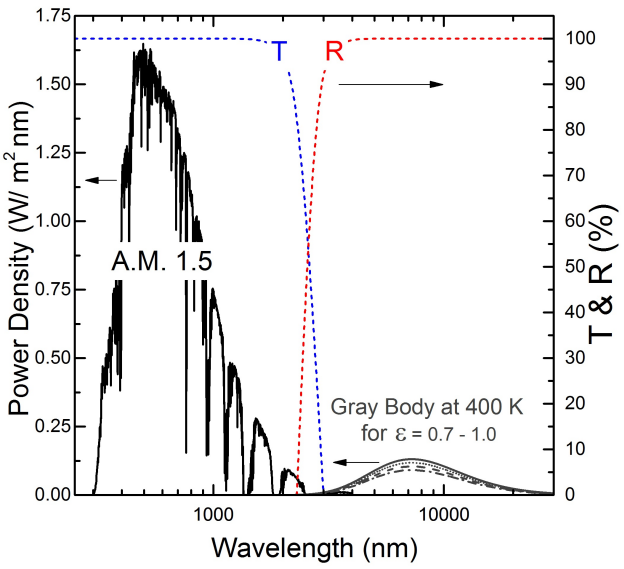

FIG. 2: The solar spectrum (black line) compared with the radiative thermal spectrum of a gray body at 400 K with emittance 0.7, 0.8, 0.9, and 1.0 (gray lines). Dashed blue, and red lines stand respectively for the transmittance, and reflectance characteristics of an ideal HM.

where σ is the Stefan-Boltzmann constant, $A_{\rm teg} = A_{\rm p}+A_{\rm n}$ is the TEG foot print area (equal to sum of the p and n leg footprint areas), $T_{\rm c}$ the TEG cold side temperature $\varepsilon_{\rm pv}^{\rm up}$ the top PV cell emittance, $\varepsilon_{\rm pv}^{\rm down}$ the effective emittance between the TEG hot side. This last effective emittance can be calculated as [24]

$$\varepsilon_{\rm pv}^{\rm down} = \frac{1}{1/\varepsilon_{\rm h} + 1/\varepsilon_{\rm c} - 1} \tag{9}$$

where $\varepsilon_{\rm h}$ and $\varepsilon_{\rm c}$ are respectively the TEG hot, and cold side emittances, and where we have neglected side walls of TE legs participating in radiation exchange [25, 26].

Emittances of solar cells are reported to exhibit values that can be in general split in two groups. Silicon, GaAs, and multi-junction solar cells were showed to exhibit high emittances, ranging between 0.7 and 0.9 [27–30], while CIGS and related alloys (such as CZTS and CGS) show values between 0.2 and 0.4 [31–33]. In both cases it is fundamental to limit as much as possible the loss of $P_{\rm in}^{\rm hstepvg}$ from the top of the system by heat radiation. Actually for $T_{\rm h}$=400 K, and $\varepsilon_{\rm pv}^{\rm up}$ ranging between 0.7 and 0.9, $Q_{\rm rad}$ is ≈700-900 W/m^2, which is almost all the incoming power G. However it seems not possible to modify solar cell emittance without modify their basic structures, and thus impairing their efficiencies, therefore different solutions are needed. One possible approach comes from the HM component reported in Fig. 1. A HM is a layer or a multi-layer of materials that exhibit high optical transmittance for the solar spectrum, showing instead high reflectance for the infrared (Fig.2). The change between highly transparent, and highly reflective behaviour happens at the plasma frequency of the material free carriers [34]. During the '80s of the last century, several publications appeared suggesting Transparent Conductive Oxides (TCOs), such as In:SnO_2 (ITO) [35] and Al:ZnO (AZO) [36] as viable candidates for HMs. The recent increasing attention raised around these materials for their application as transparent conductive front contact in solar cells [37], or as spectrum splitters in hybrid PV - thermal strategies [38–40], joint with the possibility of tuning their optical properties by changing the deposition parameters [41, 42], make this solution very interesting for future development in HSTEPVG devices.
We want in addition highlight that the implementation of TCOs as front contact, is actually the reason behind the small emittances in CIGS solar cells.

Let's therefore define the HM efficiency ratio in reflecting the infrared part as

$$\eta_{\rm hm}^{\rm r} = \left[\left(\frac{\int R(\lambda){\rm d}\lambda}{\int {\rm d}\lambda}\right)_{\rm ir}\right] \tag{10}$$

where $R(\lambda)$ is the HM reflectance, and the subscript ir means that the integral is evaluated over a range of wavelengths 2500-30000 nm. Along with the HM efficiency ration in transmitting the solar spectrum defined as

$$\eta_{\rm hm}^{\rm t} = \left[\left(\frac{\int T(\lambda){\rm d}\lambda}{\int {\rm d}\lambda}\right)_{\rm sun}\right] \tag{11}$$

where $T(\lambda)$ is the HM transmittance, and the subscript sun means that the integral is evaluated over a range of wavelengths 250-2500 nm. The quality of a heat mirror or a beam splitter is often identified by the so-called figure of merit $Z_{\rm hm}$ [43] as

$$Z_{\rm hm} = \eta_{\rm hm}^{\rm t}\ \eta_{\rm hm}^{\rm r} \tag{12}$$

Thus using Eq. 10 we can define a effective emittance for the top surface of the device similarly to the case of Eq. 9

$$\varepsilon_{\rm pv}^{\rm up'} = \frac{1}{1/\varepsilon_{\rm pv}^{\rm up} + 1/\varepsilon_{\rm hm} - 1} \tag{13}$$

where $\varepsilon_{\rm hm}$ is the HM emittance that according to Kirchhoff's law is simply equal to

$$\varepsilon_{\rm hm} = 1 - \eta_{\rm hm}^{\rm r} \tag{14}$$

By means of Eq. 13, and assuming a dissipation coefficient at the TEG cold side sufficiently high so that $T_c = T_a$, Eq. 8 can be simplified as follows

$$Q_{\rm rad} = \sigma A_{\rm abs}(T_{\rm h}^4 - T_{\rm c}^4)\left(\varepsilon_{\rm pv}^{\rm tot} - \varepsilon_{\rm pv}^{\rm down}\frac{A_{\rm teg}}{A_{\rm abs}}\right) \tag{15}$$

where

$$\varepsilon_{\rm pv}^{\rm tot} = \varepsilon_{\rm pv}^{\rm up'} + \varepsilon_{\rm pv}^{\rm down} \tag{16}$$

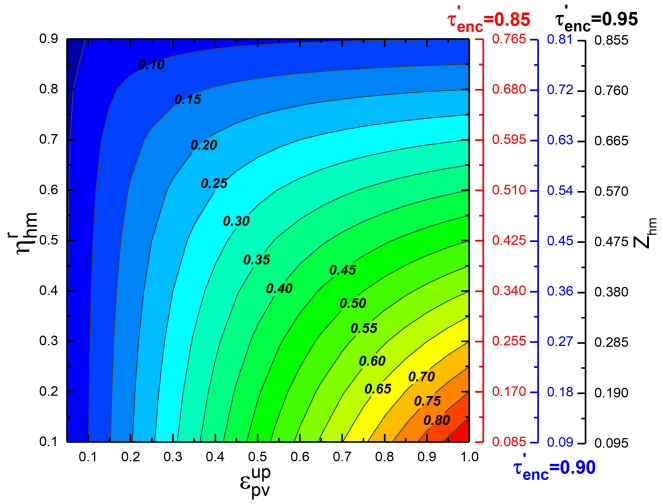

FIG. 3: Values of ε_{pv}^{tot} as simultaneous function of ε_{pv}^{up}, and η_{hm}^{r}. The TEG emittances are supposed to be ε_h=ε_c=0.07 (the emittance of copper) giving ε_{pv}^{down}=0.036 by means of Eq. 9. On the right side we report additional axis showing Z_{hm} values (obtained by Eq. 12) for τ'_{enc} = 0.85 (red axis), 0.90 (blue axis), 0.95 (black axis).

However as we will show later, in order to have high temperature differences between the TEG hot and cold sides the ratio A_{teg}/A_{abs} (often called filling factor FF) as to be very small. Therefore the last term in the brackets of Eq. 15 can be neglected without affecting the results, as often done in several previous studies [5, 19, 25]. Thus

$$Q_{rad} = \varepsilon_{pv}^{tot}\sigma A_{abs}(T_h^4 - T_c^4) \tag{17}$$

The addition of the HM also acts on the incoming power reducing the encapsulation transmittance which has to be substituted by an effective transmittance

$$\tau'_{enc} = \tau_{enc}\eta_{hm}^{t} \tag{18}$$

giving

$$\eta'_{opt} = \eta_{opt}\eta_{hm}^{t} = (1-r)(1-s)\tau'_{enc} \tag{19}$$

In Fig.3 we report the relation between ε_{pv}^{tot}, and the two parameters ε_{pv}^{up} and η_{hm}^{r}. The picture also shows the corresponding Z_{hm} values for values of τ'_{enc} equal to 0.85, 0.90, and 0.95.

Now we can define the equation for the heat flowing through the TEG that can be written as

$$Q_{te} = S_{pn}T_h I + \frac{T_h - T_c}{R_p^{th} + R_n^{th}} - \frac{I^2(R_p^{el} + R_n^{el})}{2} \tag{20}$$

where S_{pn} is the seebeck coefficient of the TEG couple, I the current flowing in TEG, R_p^{th} and R_n^{th} respectively the p and n leg thermal resistances, and R_p^{el} and R_n^{el} respectively the p and n leg electrical resistances.

Therefore by means of Eqs. 3, 7, and 17 - 20, Eq. 1 can be written for the HSTEPVG case as

$$(1-\eta_{pv})\eta'_{opt}\gamma_{op}\eta_{op}GA_{abs} = S_{pn}T_h I + \frac{T_h - T_c}{R_p^{th} + R_n^{th}} - \frac{I^2(R_p^{el} + R_n^{el})}{2} + \frac{T_h - T_c}{R_{con}} + \varepsilon_{pv}^{tot}\sigma A_{abs}(T_h^4 - T_c^4) \tag{21}$$

B. HSTEPVG efficiency and Energetic Convenience Index

As reported in Fig. 1 the PV and TEG part are thermally coupled but electrically separated. Therefore the HSTEPVG overall electrical power is simply the sum of the PV and the TEG output power

$$P_{hstepvg} = P_{pv} + P_{teg} \tag{22}$$

Consequently the overall efficiency is

$$\eta_{hstepvg} = \frac{P_{pv} + P_{teg}}{\gamma_{op}GA_{abs}} = \eta_{pv} + \eta_{te} \tag{23}$$

where η_{pv} is the PV efficiency at concentration ratio γ_{op}, and temperature T_h. The solar cell efficiency dependency on these parameters is reported in literature to be positive and logarithmic for optical concentration [44], and negative and linear for temperature [45–47]. Thus one can write

$$\eta_{pv} = \eta_{pv}^{0} + \eta_{pv-cond} \tag{24}$$

where η_{pv}^{0} is the PV efficiency at standard test conditions [48] (γ_{op}=1, and T_h=300 K), and

$$\eta_{pv-cond} = \eta_{pv}^{0}[\beta_{op}\log\gamma_{op} - \beta_{th}(T_h - T_a)] \tag{25}$$

where β_{op}, and β_{th} are respectively the optical concentration coefficient, and the slope of η_{pv} versus temperature. It is important to clarify that since solar cell temperature sensitivity is due to carrier recombination, and since optical concentration modifies carrier injection (consequently

recombination rates) it follows that the temperature coefficient $\beta_{\rm th}$ should be modelled as a function of the concentration ratio $\gamma_{\rm op}$. Actually it is well known that solar cell temperature sensitivity is smaller in the case of optically concentrated systems. In literature this dependency is reported to be logarithmic [49] therefore

$$\beta_{\rm th} = \beta^0_{\rm th}(1 - \zeta \log \gamma_{\rm op}) \tag{26}$$

with $\beta^0_{\rm th}$ the temperature coefficient at no optical concentration, and ζ the coefficient of $\beta_{\rm th}$ versus $\gamma_{\rm op}$.
In this work we use fixed values of $\beta_{\rm op}$=0.097 [44], and ζ=0.265 [49], while we consider variable the temperature coefficient at no optical concentration $\beta^0_{\rm th}$ in order to take into account different kind of solar cells.

The other component of the right side of Eq. 23 is the TEG efficiency that can be obtained as follows

$$\eta_{\rm te} = \frac{P_{\rm te}}{\gamma_{\rm op} G A_{\rm abs}} = \frac{I[S_{\rm pn}(T_{\rm h} - T_{\rm c}) - I R_{\rm i}]}{\gamma_{\rm op} G A_{\rm abs}} \tag{27}$$

where

$$R_{\rm i} = R^{\rm el}_{\rm p} + R^{\rm el}_{\rm n} \tag{28}$$

Following Chen [19] the TEG efficiency can also be expressed as

$$\eta_{\rm te} = \eta_{\rm teg}\eta_{\rm ot} \tag{29}$$

where $\eta_{\rm teg}$ is the thermoelectric efficiency

$$\eta_{\rm teg} = \frac{T_{\rm h} - T_{\rm c}}{T_{\rm h}} \frac{\sqrt{1 + Z_{\rm pn} T_{\rm m}} - 1}{\sqrt{1 + Z_{\rm pn} T_{\rm m}} + \frac{T_{\rm c}}{T_{\rm h}}} \tag{30}$$

with $Z_{\rm pn}$ the TEG figure of merit given by

$$Z_{\rm pn} = \frac{S^2_{\rm pn}}{(\sqrt{\kappa_{\rm p}\rho_{\rm p}} + \sqrt{\kappa_{\rm n}\rho_{\rm n}})^2} \tag{31}$$

where α, ρ, and κ are respectively the Seebeck coefficient, the electrical resistivity, and the thermal conductivity of the p and n thermoelectric material composing the TEG, and $T_{\rm m}$ the average temperature

$$T_{\rm m} = \frac{T_{\rm h} + T_{\rm c}}{2} \tag{32}$$

The relationship between $R_{\rm p}$ and $\rho_{\rm p}$ is simply

$$R^{\rm el}_{\rm p} = \frac{\rho_{\rm p} L_{\rm p}}{A_{\rm p}} \tag{33}$$

where $A_{\rm p}$ and $L_{\rm p}$ are respectively the thermoelectric p leg cross-sectional area, and length. Same equation is valid for the n leg.
The other factor in Eq. 29 is the opto-thermal efficiency, which is the system efficiency in converting the incoming solar power into heat actually flowing through the TEG

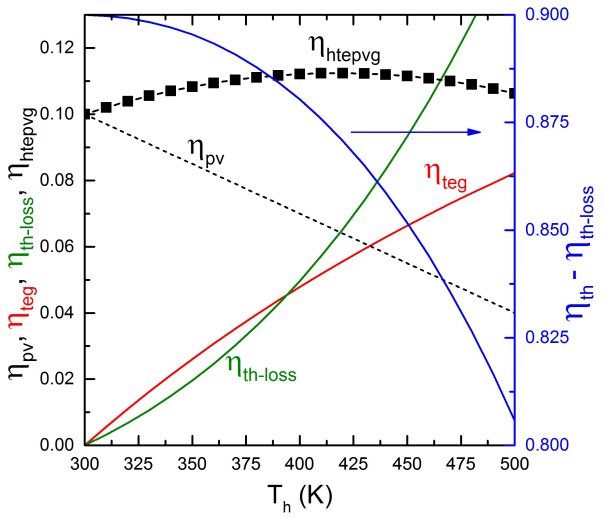

FIG. 4: Various components of the hybrid device efficiency $\eta_{\rm hstepvg}$, as described in Eq. 35 versus $T_{\rm h}$.

$$\eta_{\rm ot} = \frac{Q_{\rm te}}{\gamma_{\rm op} G A_{\rm abs}} = \eta_{\rm th} - \eta_{\rm th-loss} \tag{34}$$

with $\eta_{\rm th}$ and $\eta_{\rm th-loss}$ defined respectively by Eqs. 4 and 6.

Now using Eqs. 24, 29, and 34 we can rewrite Eq. 23 as

$$\eta_{\rm hstepvg} = \eta^0_{\rm pv} + [\eta_{\rm teg}(\eta_{\rm th} - \eta_{\rm th-loss}) + \eta_{\rm pv-cond}] \tag{35}$$

An example of the interplay between the components of Eq. 35 is reported in Fig. 4.

We can now introduce an *Energetic Convenience Index* (*EnCI*) as

$$EnCI = \eta_{\rm teg}(\eta_{\rm th} - \eta_{\rm th-loss}) + \eta_{\rm pv-cond} = \eta_{\rm te} + \eta_{\rm pv-cond} \tag{36}$$

which define the efficiency gain due to the TEG addition, and thus the convenience of the coupling from an energetic point of view. Actually an *EnCI* greater than zero means an increased efficiency for the HSTEPVG respect to the sole PV case. It follows that the maximization of *EnCI* means also maximization the HSTEPVG efficiency. Controversially an *EnCI* smaller than zero means a efficiency loss in comparison with the sole PV case.
In the following section we will report the conditions for which the maximum *EnCI* is found, and we will analyze the parameters useful to such a maximization.

III. MAXIMUM *ENCI*

Lets assume now the case for which the HSTEPVG system works under vacuum within the encapsulation. In this case we can neglect the convective contribution to thermal losses, thus $Q_{\rm con}$=0.

Furthermore hereafter we will also assume that the cold side is taken at fixed temperature equal to T_a=300 K. This is compatible with what recently reported for similar STEG systems [5]. With these assumptions *EnCI* equals

$$EnCI = \frac{I[S_{pn}(T_h - T_a) - IR_i]}{\gamma_{op} G A_{abs}} + \beta_{op}\log\gamma_{op} - \beta_{th}(T_h - T_a) \quad (37)$$

We want now to find and analyse the conditions for the maximization of Eq. 37. Following Chen [19] we can usefully introduce the following parameters

$$\gamma_{th,p} = \frac{A_{abs}}{A_p}, \gamma_{np} = \frac{A_n}{A_p}, Y = \frac{IL}{A_p} \quad (38)$$

which give the following equations for *EnCI*, and for the energy balance of Eq. 21

$$EnCI = \frac{Y[S_{pn}(T_h - T_a) - Y(\rho_p + \rho_n/\gamma_{np})]}{\gamma_{op} G \gamma_{th,p} L} + \beta_{op}\log\gamma_{op} - \beta_{th}(T_h - T_a) \quad (39)$$

$$(1 - \eta^0_{pv}(1 + (\beta_{op}\log\gamma_{op} - \beta_{th}(T_h - T_a))))\eta'_{opt}\eta_{op}\gamma_{op} G \gamma_{th,p} = S_{pn} T_h \frac{Y}{L} + (k_p + k_n\gamma_{np})\frac{T_h - T_a}{L} - \frac{Y^2}{2L}(\rho_p + \rho_n/\gamma_{np}) + \varepsilon^{tot}_{pv}\sigma\gamma_{th,p}(T_h^4 - T_a^4) \quad (40)$$

where we have made explicit all the components of η_{pv} using Eqs. 24 and 25.

Now using the Lagrangian multiplier method is then possible to find the conditions for the maximization of *EnCI* as function of T_h, Y, L, $\gamma_{th,p}$, and γ_{pn}. The analysis (reported entirely within Appendix A) gives the following results

1. The load matching condition for the TEG part of the HSTEPVG at maximum efficiency is the same as for the maximum output power and is equal to

$$\frac{R_l}{R_i} = \sqrt{1 + Z_{pn}T_m} \quad (41)$$

where R_l is the load electrical resistance.

2. The maximum efficiency is reached when the ratio between the n and p leg areas γ_{pn} equals

$$\gamma_{pn} = \sqrt{\frac{\rho_n\kappa_p}{\rho_p\kappa_n}} \quad (42)$$

where we assumed that the value of L is the same for both legs.

3. The optimal value of T_h is independent from the geometrical parameters $\gamma_{th,p}$, γ_{pn}, L, and the number of leg pairs N_c, and can be determined by the following equation

$$\frac{(1 - \eta_{pv})\eta'_{opt}\eta_{op}\gamma_{op} G - \epsilon^{tot}_{pv}\sigma(T_h^4 - T_a^4)}{4\epsilon^{tot}_{pv}\sigma T_h^4 - \eta^0_{pv}\beta_{th}\eta_{op}\gamma_{op} G T_h(\eta'_{opt} - \frac{1}{\eta_{teg}})} = \frac{\sqrt{1 + Z_{pn}T_m} + T_a/T_h}{\frac{T_a\sqrt{1+Z_{pn}T_m}}{T_h - T_a} + \frac{1}{2}} \quad (43)$$

Therefore once the system optical properties, and the value of $Z_{pn}T_m$ are set, the optimal temperature and the *EnCI* are defined.

4. The optimal geometrical proportion for the thermoelectric legs is

$$\gamma_{th}L = (k_p + k_n\gamma_{np}) \frac{T_a\sqrt{1 + Z_{pn}T_m} + (T_h - T_a)/2}{T_m\left[4\epsilon^{tot}_{pv}\sigma T_h^3 - \eta^0_{pv}\beta_{th}\gamma_{op} G(\eta'_{opt}\eta_{op} - \frac{1}{\eta_{teg}})\right]} \quad (44)$$

In Fig. 5a we report the values of maximum *EnCi* as a function of β^0_{th}, for different values of η^0_{pv} and γ_{op}. We suppose to have a HM leading to τ'_{enc}=0.90, and ε^{tot}_{pv}=0.10, and a TEG with $Z_{pn}T_m$=1. The values of β^0_{th} are taken instead in in the range 0.001 - 0.005 K^{-1} as normally done for PV materials with energy gap within 0.5 and 2.5 eV [45].
Obviously the values of *EnCi* are grater for small β^0_{th} in all the cases considered, because to a small sensitivity with temperature of the PV part. The graph also shows higher values of *EnCi* in case of small η^0_{pv} because to the impact on η_{th}. Actually a small η^0_{pv} means a greater η_{th} and thus an higher η_{op} as shown by Eqs. 4 and 34. Also optical concentration impacts positively on *EnCi* especially for its influence on recombination through β_{th} (Eq.26).

Nonetheless a higher value of *EnCi* means also a higher optimal temperature T_h as shown by Fig. 5b. From this graph is possible to understand how most of the maximum *EnCi* higher than 0.04 are hardly implementable since correspond to temperature above 450 K. At these

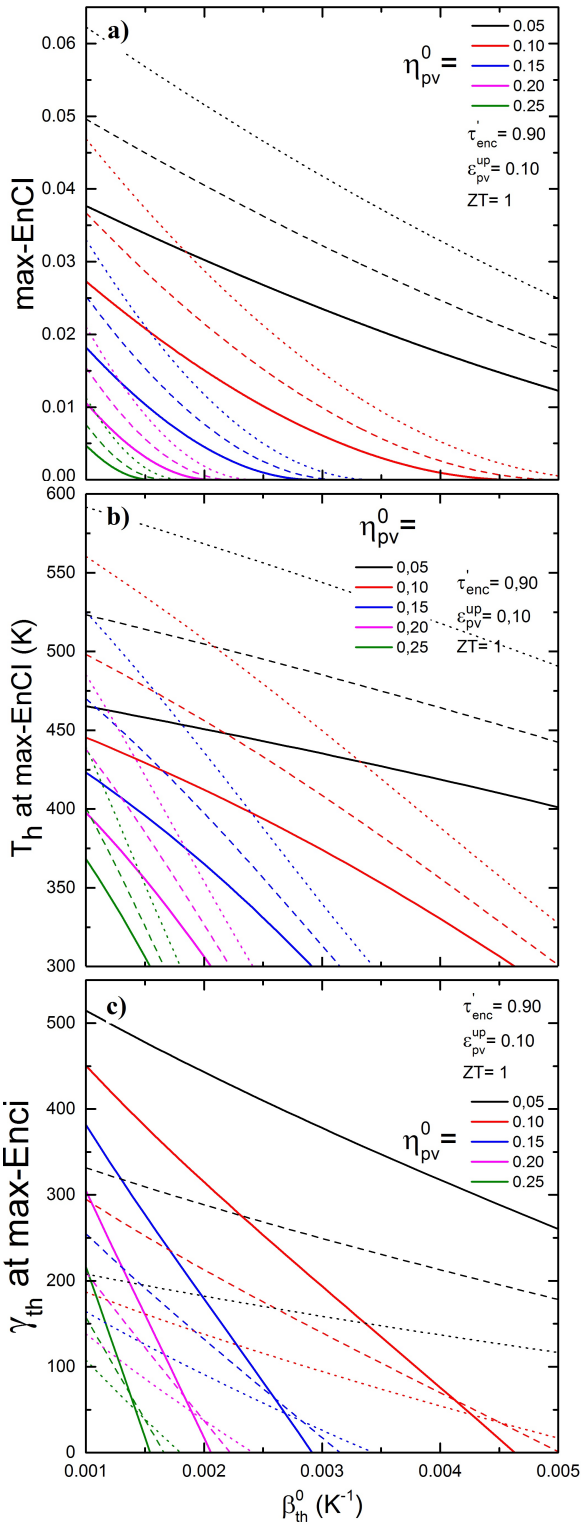

FIG. 5: Maximum *EnCi* (a), $T_{\rm h}$ at maximum *EnCi* (b),and $\gamma_{\rm th}$ at maximum *EnCi* (c) as a function of $\beta^0_{\rm th}$. Different values of $\eta^0_{\rm pv}$ (see legend of colors), and $\gamma_{\rm op}$=1 (full lines), $\gamma_{\rm op}$=2 (dashed lines), $\gamma_{\rm op}$=4 (dotted lines) are considered. The other relevant parameters are $\tau'_{\rm enc}$=0.90, $\varepsilon^{\rm up}_{\rm pv}$=0.10, and $Z_{\rm pn}T_{\rm m}$=1.

temperatures several issues as ohmic contact and semiconductors degradation, dopant diffusion, and others can lead to irreversible degradation of the PV part [50]. Even if relevant progresses on these technological limitations has been achieved in the field of high-temperature solar cells, especially for near-sun space missions [51–54], and for thermophotovoltaic applications [2, 55], the applicability of high working temperatures has to be evaluated depending on the kind of PV cell implemented.

Fig. 5c reports instead the values of $\gamma_{\rm th}$ corresponding to the maximum *EnCi*. As expected higher the optimal temperature (and consequently the maximum *EnCi*) higher the optimal $\gamma_{\rm th}$. In general for all the cases considered $\gamma_{\rm th}$ is greater than 100. This means that with a TEG having the same footprint area for the p and n legs ($\gamma_{\rm np}$=1) the TEG filling factor $FF_{\rm teg}$ (equal to $A_{\rm teg}/A_{\rm abs} = (1+\gamma_{\rm np})/\gamma_{\rm th}$) is smaller than 0.02 well justifying the assumption done for Eq. 17. Therefore as already shown elsewhere [56] the optimal TEG design for HSTEPVG applications is far from that normally implemented in commercial TEGs. In fact for actual commercially available TEGs the filling factors are normally around 0.8 - 0.9 which are at least two order of magnitudes higher than those needed for hybrid applications. This evidence calls for the need of novel and specifics TEGs industrial productions to be hybridized with solar cells.

IV. RESULTS AND DISCUSSION

In this section we want discuss about the values of *EnCi* at a fixed working temperature equal to 450 K, as a function of the optical concentration $\gamma_{\rm op}$, the thermoelectric figure of merit $Z_{\rm pn}T_{\rm m}$, and the HM properties. The temperature of 450 K has been chosen in view of recent developments of high temperature solar cells capable of working at such high temperature without damaging [53], and for the compatibility of this temperature with Bi_2Te_3 based TEGs, which are the most established thermoelectric material. For the sake of clarity in this section we also fixed $\beta^0_{\rm th}$ to a medium value of 0.002 K^{-1}.

Fig. 6 reports the value of *EnCi* at 450 K as a function of $\gamma_{\rm op}$ for different values of $\eta^0_{\rm pv}$. As shown in the graph *EnCi* increases considerably increasing the optical concentration because to the influence of the optical concentration on recombination through $\beta_{\rm th}$. For values of $\eta^0_{\rm pv}$ higher than 0.1 *EnCi* starts to become positive at different $\gamma_{\rm op}$, defining a minimum optical concentration ratio for which thermoelectric hybridization increases the efficiency of the sole PV case.

In Fig. 7 is depicted instead the behavior of *EnCi* versus $Z_{\rm pn}T_{\rm m}$. Obviously *EnCi* increases increasing $Z_{\rm pn}T_{\rm m}$ for all the values of $\eta^0_{\rm pv}$ considered. However

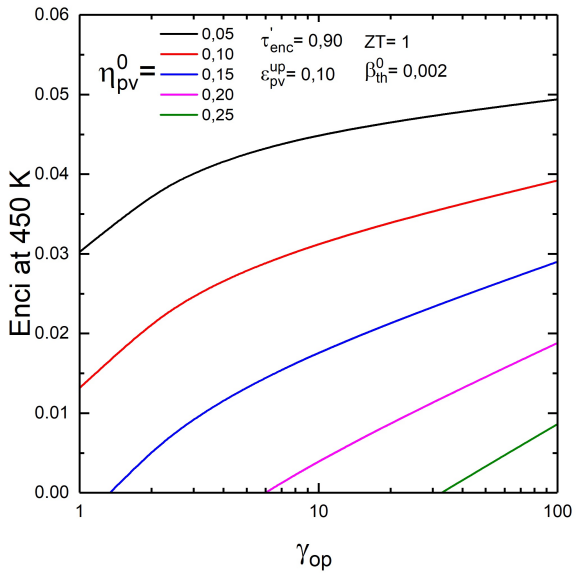

FIG. 6: Values of *EnCi* at 450 K versus $\gamma_{\rm op}$ for different values of $\eta^0_{\rm pv}$ (see legend of colors). The taken parameters are $\beta^0_{\rm th}$=0.002, $\tau'_{\rm enc}$=0.90, $\varepsilon^{\rm up}_{\rm pv}$=0.10, and $Z_{\rm pn}T_{\rm m}$=1.

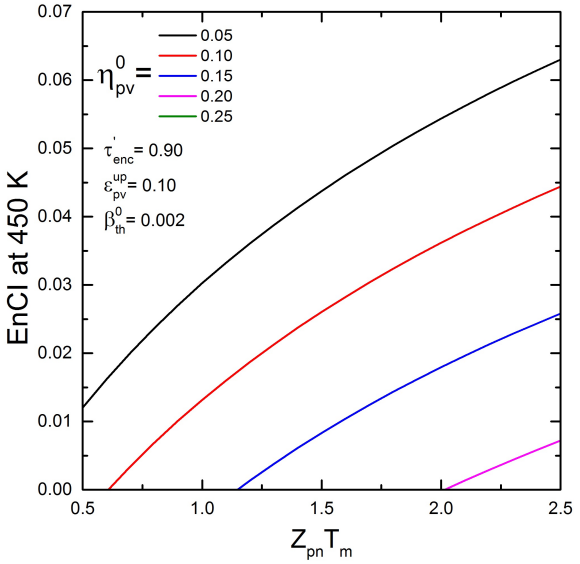

FIG. 7: Values of *EnCi* at 450 K versus $Z_{\rm pn}T_{\rm m}$ for different values of $\eta^0_{\rm pv}$ (see legend of colors). Other parameters are $\beta^0_{\rm th}$=0.002, $\tau'_{\rm enc}$=0.90, $\varepsilon^{\rm up}_{\rm pv}$=0.10, and $\gamma_{\rm op}$=1.

the slope of this increase is higher for smaller $\eta^0_{\rm pv}$ and viceversa. The reason of this trend is due to the fact that the efficiency in converting the solar input into heat flowing trough the TEG ($\eta_{\rm th}$) is higher for smaller $\eta^0_{\rm pv}$.

Finally in Fig. 8 we show the dependency of *EnCi* on $\epsilon^{\rm pv}_{\rm tot}$. In this case *EnCi* increases linearly decreasing the PV total emittance. However as also showed in Fig. 4 a change of $\epsilon^{\rm pv}_{\rm tot}$ needs a change also of $Z_{\rm hm}$. In particular, to achieve small values of $\epsilon^{\rm pv}_{\rm tot}$ which are beneficial for *EnCi* high value of $Z_{\rm hm}$ are needed. Therefore the development of efficient HMs is a fundamental condition for the achievement of efficient HSTEPVG.

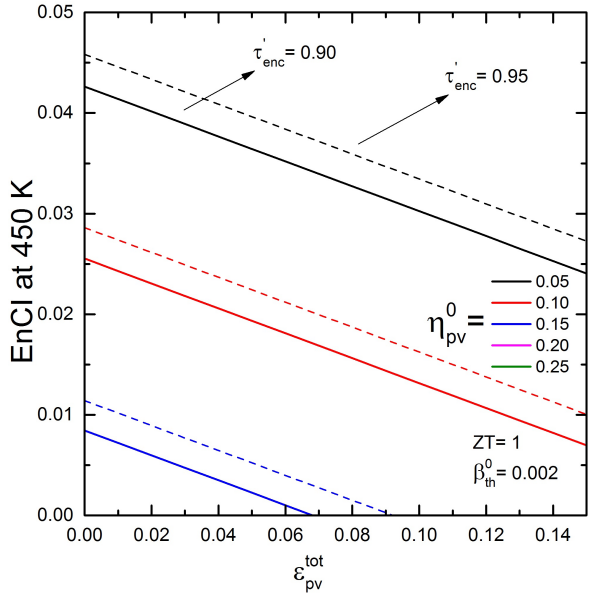

FIG. 8: Values of *EnCi* at 450 K versus $\varepsilon^{\rm tot}_{\rm pv}$ for different values of $\eta^0_{\rm pv}$ (see legend of colors), and for $\tau'_{\rm enc}$=0.90 (full lines), and $\tau'_{\rm enc}$=0.95 (dashed lines). Other parameters are $\beta^0_{\rm th}$=0.002, $Z_{\rm pn}T_{\rm m}$=1, and $\gamma_{\rm op}$=1.

V. CONCLUSION

In this paper we have reported a model for the determination of the theoretical efficiency of HSTEPVG systems. The potential of this novel kind of devices has been studied by analyzing the influence of the main parameters on the index *EnCi* representing the efficiency gain compare to the sole PV case. The analysis showed the existence of an optimal operational temperature, leading to the maximum *EnCi* compromising the efficiency increase of the TEG part with the PV temperature sensitivity. Interestingly enough the optimal temperature is not influenced by the TEG geometrical dimensions and number of legs, but is set once the system optical properties and the TEG figure of merit are known.

The model results demonstrated the possibility of reaching *EnCi* value of 4-5% for small optical concentrations, and for state of the art parameters. The thermoelectric hybridization were found to be more effective in the case of low efficiency solar cells. We also showed the beneficial effect of high optical concentration, leading to higher *EnCi* because to the smaller temperature sensitivity of the PV stage. Finally the work also revealed the fundamental importance of the optical properties of the encapsulation, along with the need of better solution for the development of solar cells able to stand high operational temperature.

It is worth clarifying that *EnCi* indicates only the ener-

getic convenience of solar cell thermoelectric hybridization, without taking into account economical effectiveness. This latter is a different and complicated matter that deserves attention even if it is far from the scope of this paper. Recently few works exploring this subject has been published [57–59] showing how economical convenience for thermoelectric hybridization compare to the sole PV case can be found for sufficiently high optical concentration (≥ 10). Actually for this case no additional costs are needed for the heat exchanger section, which is known to have a significant impact on the system cost [60]. The convenience was shown to increase increasing the thermal concentration for the thermoelectric stage, therefore reducing the amount of thermoelectric material needed.

VI. ACKNOWLEDGEMENTS

This project has received funding from the European Union's Horizon 2020 research and innovation programme under the Marie Skłodowska-Curie grant agreement No. 745304.

APPENDIX A FULL MATHEMATICAL DERIVATION

Using the Lagrangian method we have the following set of six equations

$$EnCI(T_\mathrm{h},Y,L,\gamma_\mathrm{th,p},\gamma_\mathrm{np}) = \frac{Y[S_\mathrm{pn}(T_\mathrm{h}-T_\mathrm{a})-Y(\rho_\mathrm{p}+\rho_\mathrm{n}/\gamma_\mathrm{np})]}{\gamma_\mathrm{op}G\gamma_\mathrm{th,p}L} + \eta^0_\mathrm{pv}[\beta_\mathrm{op}\log\gamma_\mathrm{op}-\beta_\mathrm{th}(T_\mathrm{h}-T_\mathrm{a})] + \lambda[S_\mathrm{pn}T_\mathrm{h}\frac{Y}{L}+(k_\mathrm{p}+k_\mathrm{n}\gamma_\mathrm{np})\frac{T_\mathrm{h}-T_\mathrm{a}}{L}-\frac{Y^2}{2L}(\rho_\mathrm{p}+\rho_\mathrm{n}/\gamma_\mathrm{np})+\varepsilon^\mathrm{tot}_\mathrm{pv}\sigma\gamma_\mathrm{th,p}(T^4_\mathrm{h}-T^4_\mathrm{a}) - (1-(\eta^0_\mathrm{pv}(1+(\beta_\mathrm{op}\log\gamma_\mathrm{op}-\beta_\mathrm{th}(T_\mathrm{h}-T_\mathrm{a})))))\eta'_\mathrm{opt}\eta_\mathrm{op}\gamma_\mathrm{op}G\gamma_\mathrm{th,p}] \quad (A.1)$$

$$0 = \frac{\partial EnCi}{\partial\gamma_\mathrm{th,p}} = -\frac{Y[S_\mathrm{pn}(T_\mathrm{h}-T_\mathrm{a})-Y(\rho_\mathrm{p}+\rho_\mathrm{n}/\gamma_\mathrm{np})]}{\gamma_\mathrm{op}G\gamma^2_\mathrm{th,p}L} + \lambda[\varepsilon^\mathrm{tot}_\mathrm{pv}\sigma(T^4_\mathrm{h}-T^4_\mathrm{a})-(1-(\eta^0_\mathrm{pv}(1+(\beta_\mathrm{op}\log\gamma_\mathrm{op} - \beta_\mathrm{th}(T_\mathrm{h}-T_\mathrm{a})))))\eta'_\mathrm{opt}\eta_\mathrm{op}\gamma_\mathrm{op}G] \quad (A.2)$$

$$0 = \frac{\partial EnCi}{\partial\gamma_\mathrm{np}} = \frac{Y^2(\rho_\mathrm{n}/\gamma^2_\mathrm{np})]}{\gamma_\mathrm{op}G\gamma^2_\mathrm{th,p}L} + \lambda\left[k_\mathrm{n}\frac{T_\mathrm{h}-T_\mathrm{a}}{L}+\frac{Y^2}{2L}\left(\frac{\rho_\mathrm{n}}{\gamma^2_\mathrm{np}}\right)\right] \quad (A.3)$$

$$0 = \frac{\partial EnCi}{\partial Y} = \frac{S_\mathrm{pn}(T_\mathrm{h}-T_\mathrm{a})-2Y(\rho_\mathrm{p}+\rho_\mathrm{n}/\gamma_\mathrm{np})}{\gamma_\mathrm{op}G\gamma_\mathrm{th,p}L} + \lambda\left[S_\mathrm{pn}T_\mathrm{h}\frac{1}{L}-\frac{Y}{L}(\rho_\mathrm{p}+\rho_\mathrm{n}/\gamma_\mathrm{np})\right] \quad (A.4)$$

$$0 = \frac{\partial EnCi}{\partial T_\mathrm{h}} = \frac{YS_\mathrm{pn}}{\gamma_\mathrm{op}G\gamma_\mathrm{th,p}L} - \eta^0_\mathrm{pv}\beta_\mathrm{th} + \lambda[S_\mathrm{pn}\frac{Y}{L}+(\kappa_\mathrm{p}+\kappa_\mathrm{n}\gamma_\mathrm{np})\frac{1}{L}+4\varepsilon^\mathrm{tot}_\mathrm{pv}\sigma\gamma_\mathrm{th,p}T^3_\mathrm{h} - \eta^0_\mathrm{pv}\beta_\mathrm{th}\eta'_\mathrm{opt}\eta_\mathrm{op}\gamma_\mathrm{op}G\gamma_\mathrm{th,p}] \quad (A.5)$$

$$0 = \frac{\partial EnCi}{\partial L} = -\frac{Y[S_\mathrm{pn}(T_\mathrm{h}-T_\mathrm{a})-Y(\rho_\mathrm{p}+\rho_\mathrm{n}/\gamma_\mathrm{np})]}{\gamma_\mathrm{op}G\gamma_\mathrm{th,p}L^2} + \lambda[-S_\mathrm{pn}T_\mathrm{h}\frac{Y}{L^2}-(\kappa_\mathrm{p}+\kappa_\mathrm{n}\gamma_\mathrm{np})\frac{T_\mathrm{h}-T_\mathrm{a}}{L^2} + \frac{Y^2}{2L^2}(\rho_\mathrm{p}+\rho_\mathrm{n}/\gamma_\mathrm{np})] \quad (A.6)$$

From Eqs. A.4, and A.6, along with Eq. 31 we obtain the following equation for Y

$$Y = \frac{(\kappa_\mathrm{p}+\kappa_\mathrm{n}\gamma_\mathrm{np})(T_\mathrm{h}-T_\mathrm{a})\left(\sqrt{1+Z_\mathrm{pn}T_\mathrm{m}}-1\right)}{S_\mathrm{pn}T_\mathrm{m}} \quad (A.7)$$

where $Z_\mathrm{pn}T_\mathrm{m}$ can be written as

$$Z_\mathrm{pn}T_\mathrm{m} = \frac{S^2_\mathrm{pn}T_\mathrm{m}}{(\rho_\mathrm{p}+\rho_\mathrm{n}/\gamma_\mathrm{np})(\kappa_\mathrm{p}+\kappa_\mathrm{n}\gamma_\mathrm{np})} \quad (A.8)$$

Eq. A.7 is the exactly the same equation which stands also for the STEG case [19]. Therefore it follows that the conclusions valid for STEGs regarding this equation can be drawn also for HSTEPVGs. In particular it follows that the ratio between the TEG leg areas which maximizes $Z_\mathrm{pn}T_\mathrm{m}$ is

$$\gamma_\mathrm{pn} = \sqrt{\frac{\rho_\mathrm{n}\kappa_\mathrm{p}}{\rho_\mathrm{p}\kappa_\mathrm{n}}} \quad (A.9)$$

and that the load matching condition can be written as

$$\frac{R_\mathrm{l}}{R_\mathrm{i}} = \sqrt{1+Z_\mathrm{pn}T_\mathrm{m}} \quad (A.10)$$

Now we can use Eqs. A.7 and A.8 to re-write the energy balance of Eq. 40 in terms of Y as follows

$$\left[(1-\eta_{\mathrm{pv}})\eta'_{\mathrm{opt}}\eta_{\mathrm{op}}\gamma_{\mathrm{op}}G-\varepsilon^{\mathrm{tot}}_{\mathrm{pv}}\sigma(T_{\mathrm{h}}^4-T_{\mathrm{a}}^4)\right]\gamma_{\mathrm{th,p}}L = (k_{\mathrm{p}}+k_{\mathrm{n}}\gamma_{\mathrm{np}})\frac{(T_{\mathrm{h}}-T_{\mathrm{a}})T_{\mathrm{h}}\sqrt{1+Z_{\mathrm{pn}}T_{\mathrm{m}}}\left(\sqrt{1+Z_{\mathrm{pn}}T_{\mathrm{m}}}+T_{\mathrm{a}}/T_{\mathrm{h}}\right)}{T_{\mathrm{m}}\left(\sqrt{1+Z_{\mathrm{pn}}T_{\mathrm{m}}}+1\right)} \quad \text{(A.11)}$$

From Eqs. A.4, and A.5 we have instead

$$\frac{S_{\mathrm{pn}}(T_{\mathrm{h}}-T_{\mathrm{a}})-2Y(\rho_{\mathrm{p}}+\rho_{\mathrm{n}}/\gamma_{\mathrm{np}})}{YS_{\mathrm{pn}}-\eta^0_{\mathrm{pv}}\beta_{\mathrm{th}}\gamma_{\mathrm{op}}G\gamma_{\mathrm{th,p}}L} = \frac{S_{\mathrm{pn}}T_{\mathrm{h}}-Y\left(\rho_{\mathrm{p}}+\rho_{\mathrm{n}}/\gamma_{\mathrm{np}}\right)}{S_{\mathrm{pn}}Y+\left(\kappa_{\mathrm{p}}+\kappa_{\mathrm{n}}\gamma_{\mathrm{np}}\right)+4\varepsilon^{\mathrm{tot}}_{\mathrm{pv}}\sigma\gamma_{\mathrm{th,p}}T_{\mathrm{h}}^3L-\eta^0_{\mathrm{pv}}\beta_{\mathrm{th}}\eta'_{\mathrm{opt}}\eta_{\mathrm{op}}\gamma_{\mathrm{op}}G\gamma_{\mathrm{th,p}}L} \quad \text{(A.12)}$$

which leads to

$$4\varepsilon^{\mathrm{tot}}_{\mathrm{pv}}\sigma\gamma_{\mathrm{th,p}}T_{\mathrm{h}}^3L-\eta^0_{\mathrm{pv}}\beta_{\mathrm{th}}\eta'_{\mathrm{opt}}\eta_{\mathrm{op}}\gamma_{\mathrm{op}}G\gamma_{\mathrm{th,p}}L = \frac{\left[YS_{\mathrm{pn}}-\eta^0_{\mathrm{pv}}\beta_{\mathrm{th}}\gamma_{\mathrm{op}}G\gamma_{\mathrm{th,p}}L\right]\left[S_{\mathrm{pn}}T_{\mathrm{h}}-Y(\rho_{\mathrm{p}}+\rho_{\mathrm{n}}/\gamma_{\mathrm{np}})\right]}{S_{\mathrm{pn}}(T_{\mathrm{h}}-T_{\mathrm{a}})-2Y(\rho_{\mathrm{p}}+\rho_{\mathrm{n}}/\gamma_{\mathrm{np}})}$$

$$-S_{\mathrm{pn}}Y-\left(\kappa_{\mathrm{p}}+\kappa_{\mathrm{n}}\gamma_{\mathrm{np}}\right) = \left(\kappa_{\mathrm{p}}+\kappa_{\mathrm{n}}\gamma_{\mathrm{np}}\right)\frac{T_{\mathrm{a}}\sqrt{1+Z_{\mathrm{pn}}T_{\mathrm{m}}}+(T_{\mathrm{h}}-T_{\mathrm{a}})/2}{T_{\mathrm{m}}}-\frac{\eta^0_{\mathrm{pv}}\beta_{\mathrm{th}}\gamma_{\mathrm{op}}G\gamma_{\mathrm{th,p}}L}{\eta_{\mathrm{teg}}} \quad \text{(A.13)}$$

where

$$\frac{1}{\eta_{\mathrm{teg}}} = \frac{S_{\mathrm{pn}}T_{\mathrm{h}}-Y(\rho_{\mathrm{p}}+\rho_{\mathrm{n}}/\gamma_{\mathrm{np}})}{S_{\mathrm{pn}}(T_{\mathrm{h}}-T_{\mathrm{a}})-2Y(\rho_{\mathrm{p}}+\rho_{\mathrm{n}}/\gamma_{\mathrm{np}})} = \frac{T_{\mathrm{h}}}{T_{\mathrm{h}}-T_{\mathrm{a}}}\frac{T_{\mathrm{a}}/T_{\mathrm{h}}+\sqrt{1+Z_{\mathrm{pn}}T_{\mathrm{m}}}}{\sqrt{1+Z_{\mathrm{pn}}T_{\mathrm{m}}}-1} \quad \text{(A.14)}$$

Now combining Eq. A.13 with Eq. A.11 we have

$$\frac{(1-\eta_{\mathrm{pv}})\eta'_{\mathrm{opt}}\eta_{\mathrm{op}}\gamma_{\mathrm{op}}G-\epsilon^{\mathrm{tot}}_{\mathrm{pv}}\sigma(T_{\mathrm{h}}^4-T_{\mathrm{a}}^4)}{4\epsilon^{\mathrm{tot}}_{\mathrm{pv}}\sigma T_{\mathrm{h}}^4-\eta^0_{\mathrm{pv}}\beta_{\mathrm{th}}\eta_{\mathrm{op}}\gamma_{\mathrm{op}}GT_{\mathrm{h}}(\eta'_{\mathrm{opt}}\eta_{\mathrm{op}}-\frac{1}{\eta_{\mathrm{teg}}})} = \frac{\sqrt{1+Z_{\mathrm{pn}}T_{\mathrm{m}}}+T_{\mathrm{a}}/T_{\mathrm{h}}}{\frac{T_{\mathrm{a}}\sqrt{1+Z_{\mathrm{pn}}T_{\mathrm{m}}}}{T_{\mathrm{h}}-T_{\mathrm{a}}}+\frac{1}{2}} \quad \text{(A.15)}$$

from which is possible to obtain the optimal working temperature T_{h}.

Finally from Eq. A.13 one can derive the leg geometrical proportion to obtain the maximum efficiency

$$\gamma_{\mathrm{th,p}}L = \left(\kappa_{\mathrm{p}}+\kappa_{\mathrm{n}}\gamma_{\mathrm{np}}\right)\frac{T_{\mathrm{a}}\sqrt{1+Z_{\mathrm{pn}}T_{\mathrm{m}}}+(T_{\mathrm{h}}-T_{\mathrm{a}})/2}{T_{\mathrm{m}}} - \frac{1}{4\varepsilon^{\mathrm{tot}}_{\mathrm{pv}}\sigma T_{\mathrm{h}}^3-\eta^0_{\mathrm{pv}}\beta_{\mathrm{th}}\gamma_{\mathrm{op}}G\left(\eta'_{\mathrm{opt}}\eta_{\mathrm{op}}-\frac{1}{\eta_{\mathrm{teg}}}\right)} \quad \text{(A.16)}$$

Finally expand the analysis to the case of TEG with multiple couples does not lead to any changes to the conclusions reported above.

Actually considering a value of N_{c} small enough to prevent later heat exchange between legs (assumption 5 in our model), and as long as the temperature of the TEG hot plate is uniform (assumption number 2 in our model) the addition of $(N_{\mathrm{c}}-1)$ couples would only change the voltage produced by the TEG (i.e. multiplied by a factor N_{c}), and the parameters Y and $\gamma_{\mathrm{th,p}}$ (i.e. divided by a factor N_{c} through A_{p}). Since none of these parameters is present in Eq. A.15 it follows that the optimal temperature, and thus the maximum efficiency do not change. Consequently also the optimal geometrical factor $\gamma_{\mathrm{th,p}}L$ remain the same, and since $\gamma_{\mathrm{th,p}}$ is divided by a factor N_{c} it follows that L has to be increased by the same factor.

[1] S. V. Boriskina, M. A. Green, K. Catchpole, E. Yablonovitch, M. C. Beard, Y. Okada, S. Lany, T. Gershon, A. Zakutayev, M. H. Tahersima, V. J. Sorger, M. J. Naughton, K. Kempa, M. Dagenais, Y. Yao, L. Xu, X. Sheng, N. D. Bronstein, J. A. Rogers, A. P. Alivisatos, R. G. Nuzzo, J. M. Gordon, D. M. Wu, M. D. Wisser, A. Salleo, J. Dionne, P. Bermel, J.-J. Greffet, I. Celanovic, M. Soljacic, A. Manor, C. Rotschild, A. Raman, L. Zhu, S. Fan, and G. Chen, "Roadmap on optical energy conversion," *Journal of Optics*, vol. 18, no. 7, p. 073004, 2016.

[2] D. M. Bierman, A. Lenert, W. R. Chan, B. Bhatia, I. Celanović, M. Soljačić, and E. N. Wang, "Enhanced photovoltaic energy conversion using thermally based spectral shaping," *Nature Energy*, vol. 1, no. 6, p. 16068, 2016.

[3] O. Dupré, R. Vaillon, and M. A. Green, "A full thermal model for photovoltaic devices," *Solar Energy*, vol. 140, pp. 73–82, 2016.

[4] R. Amatya and R. J. Ram, "Solar thermoelectric generator for micropower applications," *Journal of Electronic Materials*, vol. 39, no. 9, pp. 1735–1740, 2010.

[5] D. Kraemer, Q. Jie, K. McEnaney, F. Cao, W. Liu, L. A. Weinstein, J. Loomis, Z. Ren, and G. Chen, "Concentrating solar thermoelectric generators with a peak efficiency of 7.4%," *Nature Energy*, vol. 1, no. September, p. 16153, 2016.

[6] Y. Vorobiev, J. González-Hernández, P. Vorobiev, and L. Bulat, "Thermal-photovoltaic solar hybrid system for efficient solar energy conversion," *Solar Energy*, vol. 80, pp. 170–176, 2006.

[7] D. Kraemer, L. Hu, A. Muto, X. Chen, G. Chen, and M. Chiesa, "Photovoltaic-thermoelectric hybrid systems: A general optimization methodology," *Applied Physics Letters*, vol. 92, no. 2008, 2008.

[8] X. Ju, Z. Wang, G. Flamant, P. Li, and W. Zhao, "Numerical analysis and optimization of a spectrum splitting concentration photovoltaicthermoelectric hybrid system," *Solar Energy*, vol. 86, no. 6, pp. 1941–1954, 2012.

[9] G. Contento, B. Lorenzi, A. Rizzo, and D. Narducci, "Efficiency enhancement of a-Si and CZTS solar cells using different thermoelectric hybridization strategies," *Energy*, vol. 131, pp. 230–238, 2017.

[10] J. Zhang, Y. Xuan, and L. Yang, "Performance estimation of photovoltaic-thermoelectric hybrid systems," *Energy*, vol. 78, pp. 895–903, 2014.

[11] Y.-Y. Wu, S.-Y. Wu, and L. Xiao, "Performance analysis of photovoltaicthermoelectric hybrid system with and without glass cover," *Energy Conversion and Management*, vol. 93, pp. 151–159, 2015.

[12] R. Bjørk and K. K. Nielsen, "The performance of a combined solar photovoltaic (PV) and thermoelectric generator (TEG) system," *Solar Energy*, vol. 120, pp. 187–194, 2015.

[13] T. Cui, Y. Xuan, and Q. Li, "Design of a novel concentrating photovoltaic thermoelectric system incorporated with phase change materials," *Energy Conversion and Management*, vol. 112, pp. 49–60, 2016.

[14] Y. Da, Y. Xuan, and Q. Li, "From light trapping to solar energy utilization : A novel photovoltaic e thermoelectric hybrid system to fully utilize solar spectrum," *Energy*, vol. 95, pp. 200–210, 2016.

[15] M. Hajji, H. Labrim, M. Benaissa, A. Laazizi, H. Ez-Zahraouy, E. Ntsoenzok, J. Meot, and A. Benyoussef, "Photovoltaic and thermoelectric indirect coupling for maximum solar energy exploitation," *Energy Conversion and Management*, vol. 136, pp. 184–191, 2017.

[16] R. Lamba and S. C. Kaushik, "Modeling and performance analysis of a concentrated photovoltaic-thermoelectric hybrid power generation system," *Energy Conversion and Management*, vol. 115, pp. 288–298, 2016.

[17] B. Lorenzi, M. Acciarri, and D. Narducci, "Conditions for beneficial coupling of thermoelectric and photovoltaic devices," *Journal of Materials Research*, vol. 30, pp. 2663–2669, sep 2015.

[18] M. Telkes, "Solar thermoelectric generators," *Journal of Applied Physics*, vol. 25, no. 6, pp. 765–777, 1954.

[19] G. Chen, "Theoretical efficiency of solar thermoelectric energy generators," *Journal of Applied Physics*, vol. 109, no. 10, 2011.

[20] C. H. Henry, "Limiting efficiencies of ideal single and multiple energy gap terrestrial solar cells," *Journal of Applied Physics*, vol. 51, no. 8, p. 4494, 1980.

[21] T. Markvart, "Thermodynamics of losses in photovoltaic conversion," *Applied Physics Letters*, vol. 91, no. 6, p. 064102, 2007.

[22] L. C. Hirst and N. J. Ekins-Daukes, "Fundamental losses in solar cells," *Progress in Photovoltaics: Research and Applications*, vol. 19, pp. 286–293, may 2011.

[23] B. Lorenzi, M. Acciarri, and D. Narducci, "Experimental determination of power losses in solar cells," *arXiv:1801.04245 [physics.app-ph]*.

[24] R. Siegel, J. R. Howell, and M. P. Menguc, *Thermal Radiation Heat Transfer*. New York: Taylor & Francis, 5th ed., 2002.

[25] D. Kraemer, B. Poudel, H.-P. Feng, J. C. Caylor, B. Yu, X. Yan, Y. Ma, X. Wang, D. Wang, A. Muto, K. McEnaney, M. Chiesa, Z. Ren, and G. Chen, "High-performance flat-panel solar thermoelectric generators with high thermal concentration.," *Nature materials*, vol. 10, no. 7, pp. 422–427, 2011.

[26] K. McEnaney, D. Kraemer, Z. Ren, and G. Chen, "Modeling of concentrating solar thermoelectric generators," *Journal of Applied Physics*, vol. 110, no. 7, 2011.

[27] A. a. Hegazy, "Comparative study of the performances of four photovoltaic / thermal solar air collectors," *Energy conversion and management*, vol. 41, pp. 861–881, 2000.

[28] S. Armstrong and W. G. Hurley, "A thermal model for photovoltaic panels under varying atmospheric conditions," *Applied Thermal Engineering*, vol. 30, no. 11-12, pp. 1488–1495, 2010.

[29] L. Zhu, A. Raman, K. X. Wang, M. A. Anoma, and S. Fan, "Radiative cooling of solar cells," *Optica*, vol. 1, pp. 32–38, 2014.

[30] J. Zhang and Y. Xuan, "Investigation on the effect of thermal resistances on a highly concentrated photovoltaic-thermoelectric hybrid system," *Energy Conversion and Management*, vol. 129, pp. 1–10, 2016.

[31] M. Günthner, M. Pscherer, C. Kaufmann, and G. Motz,

"High emissivity coatings based on polysilazanes for flexible Cu(In,Ga)Se2 thin-film solar cells," *Solar Energy Materials and Solar Cells*, vol. 123, pp. 97–103, 2014.

[32] B. S. Kawakita, M. Imaizumi, K. Kibe, Y. Nakamura, and S. Nakasuka, "Flight Data of a Cu (In , Ga) Se 2 Thin-Film Solar Cell Module without a Coverglass by a Nano Satellite," *Trans. JSASS Space Tech. Japan*, vol. 7, pp. 49–53, 2009.

[33] K. Shimazaki, M. Imaizumi, and K. Kibe, "SiO2 and Al2O3/SiO2 coatings for increasing emissivity of Cu(In, Ga)Se2 thin-film solar cells for space applications," *Thin Solid Films*, vol. 516, no. 8, pp. 2218–2224, 2008.

[34] C. Kittel, *Introduction to solid state physics*. Wiley, 8th ed., 2005.

[35] J. C. Fan and F. J. Bachner, "Transparent heat mirrors for solar-energy applications.," *Applied optics*, vol. 15, no. 4, pp. 1012–1017, 1976.

[36] Z.-C. Jin, I. Hamberg, and C. G. Granqvist, "Optical properties of transparent and heat reflecting ZnO:Al films made by reactive sputtering," *Applied Physics Letters*, vol. 51, no. 3, p. 149, 1987.

[37] K. Ellmer, "Past achievements and future challenges in the development of optically transparent electrodes," *Nature Photonics*, vol. 6, pp. 809–817, nov 2012.

[38] A. G. Imenes and D. R. Mills, "Spectral beam splitting technology for increased conversion efficiency in solar concentrating systems: a review," *Solar Energy Materials & Solar Cells*, vol. 84, pp. 19–69, 2004.

[39] C. Shou, Z. Luo, T. Wang, W. Shen, G. Rosengarten, W. Wei, C. Wang, M. Ni, and K. Cen, "Investigation of a broadband TiO2/SiO2 optical thin-film filter for hybrid solar power systems," *Applied Energy*, vol. 92, pp. 298–306, 2012.

[40] K. Sibin, N. Selvakumar, A. Kumar, A. Dey, N. Sridhara, H. Shashikala, A. K. Sharma, and H. C. Barshilia, "Design and development of ITO/Ag/ITO spectral beam splitter coating for photovoltaic-thermoelectric hybrid systems," *Solar Energy*, vol. 141, pp. 118–126, 2017.

[41] M. Kumar, R. Singh, S. Nandy, A. Ghosh, S. Rath, and T. Som, "Tunable optoelectronic properties of pulsed dc sputter-deposited ZnO:Al thin films: Role of growth angle," *Journal of Applied Physics*, vol. 120, p. 015302, jul 2016.

[42] R. Sivakumar, M. Kumar, C. Sanjeeviraja, and T. Som, "Tuning electro-optical properties of pulsed dc magnetron sputtered indium tin oxide thin films: effects of pulsing frequency and annealing," *Journal of Materials Science: Materials in Electronics*, pp. 1–10, sep 2016.

[43] S. Durrani, E. Khawaja, A. Al-Shukri, and M. Al-Kuhaili, "Dielectric/Ag/dielectric coated energy-efficient glass windows for warm climates," *Energy and Buildings*, vol. 36, no. 9, pp. 891–898, 2004.

[44] J. L. Gray, "The physics of the solar cell," in *Handbook of Photovoltaic Science and Engineering* (L. Antonio and H. Steven, eds.), pp. 106–107, John Wiley and Sons Ltd, 2003.

[45] O. Dupré, R. Vaillon, and M. A. Green, "Physics of the temperature coefficients of solar cells," *Solar Energy Materials and Solar Cells*, vol. 140, pp. 92–100, 2015.

[46] P. Singh and N. Ravindra, "Temperature dependence of solar cell performancean analysis," *Solar Energy Materials and Solar Cells*, vol. 101, pp. 36–45, 2012.

[47] A. Virtuani, D. Pavanello, and G. Friesen, "Overview of Temperature Coefficients of Different Thin Film Photovoltaic Technologies," in *Proc. 25th EU PVSEC*, pp. 4248 – 4252, 2010.

[48] ASTM International, "Standard Test Method for Electrical Performance of Photovoltaic Cells Using Reference Cells Under Simulated Sunlight," tech. rep., 2016.

[49] G. Siefer and A. W. Bett, "Analysis of temperature coefficients for III-V multi-junction concentrator cells," *Progress in Photovoltaics: Research and Applications*, vol. 22, pp. 515–524, may 2014.

[50] G. a. Landis, D. Merritt, R. P. Raffaelle, and D. Scheiman, "High-temperature Solar Cell Development," *Nasa/Cp2005-213431*, vol. CP-2005-21, no. figure 2, pp. 241–247, 2005.

[51] S. Noda, K. Nagano, E. Inoue, T. Egi, T. Nakashima, N. Imawaka, M. Kanayama, S. Iwata, K. Toshima, K. Nakada, and K. Yoshino, "Development of large size dye-sensitized solar cell modules with high temperature durability," *Synthetic Metals*, vol. 159, no. 21-22, pp. 2355–2357, 2009.

[52] A. Rostami, H. Heidarzadeh, H. Baghban, M. Dolatyari, and H. Rasooli, "Thermal stability analysis of concentrating single-junction silicon and SiC-based solar cells," *Journal of Optoelectronics and Advanced Materials*, vol. 15, no. 1-2, pp. 1–3, 2013.

[53] A. Maros, S. Gangam, Y. Fang, J. Smith, D. Vasileska, S. Goodnick, M. I. Bertoni, and C. B. Honsberg, "High temperature characterization of GaAs single junction solar cells," *2015 IEEE 42nd Photovoltaic Specialist Conference, PVSC 2015*, 2015.

[54] E. E. Perl, J. Simon, J. F. Geisz, M. L. Lee, D. J. Friedman, and M. A. Steiner, "Measurements and Modeling of III-V Solar Cells at High Temperatures up to 400 °C," *IEEE Journal of Photovoltaics*, vol. 6, no. 5, pp. 1345–1352, 2016.

[55] O. Dupré, R. Vaillon, and M. Green, "Optimization of solar thermophotovoltaic systems including the thermal balance," *Proceedings of the 43rd IEEE PVSC*, no. September, pp. 1030–1033, 2016.

[56] D. Narducci and B. Lorenzi, "Challenges and Perspectives in Tandem Thermoelectric - Photovoltaic Solar Energy Conversion," *IEEE Transactions on Nanotechnology*, vol. 15, pp. 348–355, may 2016.

[57] W. G. J. H. M. V. Sark, "Feasibility of photovoltaic - Thermoelectric hybrid modules," *Appl. Energy*, vol. 88, pp. 2785–2790, 2011.

[58] W. Zhu, Y. Deng, Y. Wang, S. Shen, and R. Gulfam, "High-performance photovoltaic-thermoelectric hybrid power generation system with optimized thermal management," *Energy*, vol. 100, pp. 91–101, 2016.

[59] D. Narducci, P. Bermel, B. Lorenzi, N. Wang, and K. Yazawa, "Hybrid Solar Harvesters: Technological Challenges, Economic Issues, and Perspectives," in *Hybrid and Fully Thermoelectric Solar Harvesting*, pp. 137–151, Springer International Publishing, 2018.

[60] S. Leblanc, S. K. Yee, M. L. Scullin, C. Dames, and K. E. Goodson, "Material and manufacturing cost considerations for thermoelectrics," *Renewable and Sustainable Energy Reviews*, vol. 32, pp. 313–327, 2014.